Math Geosci
DOI 10.1007/s11004-008-9180-6

Hierarchical Geostatistical Analysis of an Experimental Stratigraphy

Ye Zhang

Received: 31 August 2006 / Accepted: 28 January 2008

Abstract A hierarchical geostatistical analysis is conducted on a high-resolution, multiscale hydraulic conductivity ($\ln K$) map, created by scaling up an experimental stratigraphy. Unlike a previous study which evaluates $\ln K$ variograms within individual depositional environments, this study analyzes deposits (or samples) that incorporate multiple depositional environments. Based on conductivity cutoffs selected from a global $\ln K$ histogram, an indicator map is created to divide the deposits into 4 categories: sand, silty sand, clayey silt, and clay (Hierarchy-I). Based on facies and facies assemblage types selected using geological criteria, two more indicator maps are created at a higher hierarchy (Hierarchy-II) to divide the deposits into 14 units and 2 units, respectively. For each sample, its experimental $\ln K$ variogram is decomposed into 4 auto- and cross-transition component variograms. The decomposition characteristics are then evaluated against the underlying heterogeneity and specific division rule. The analysis reveals that: (1) $\ln K$ cutoffs (sand contents of the physical stratigraphy) can be used to distinguish the shifts in dominant deposition mode; (2) sample univariate modes depend on the choice of hierarchical division; (3) sample variograms exhibit smooth-varying correlation structures (exponential-like variograms are observed in samples with a large variance in mean facies length); (4) the decomposition characteristics are sensitive to the division based on conductivity cutoffs, but not sensitive to the division based on depositional environment (For all samples, with appropriate division, the sample variogram is closely approximated by the sum of the cross-transition component variograms.); and (5) at the Hierarchy-II level, the 2-unit division gives similar decomposition characteristics as the 14-unit division. For the select samples, parsimony in hierarchical division is achieved at the facies assemblage scale.

Y. Zhang (✉)
Department of Geology and Geophysics, University of Wyoming, Dept. 3006, 1000 University Ave., Laramie, WY 82071, USA
e-mail: yzhang9@uwyo.edu

Keywords Geostatistics · Variogram · Experimental stratigraphy · Hierarchical decomposition

1 Introduction

Heterogeneity of hydraulic conductivity (K) controls the fate of subsurface fluid flow and solute transport. In sedimentary aquifers, it is increasingly recognized that depositional structure controls K heterogeneity. In particular, a class of deposits analyzed extensively is the alluvial or fluvial sedimentary systems. Groundwater in such deposits is commonly dominated by porous flow; thus, stochastic theories are developed to predict large scale flow/transport and their uncertainties, based on the spatial correlation and variability characteristics of natural log conductivity ($\ln K$) (Rubin 2003). However, most fluvial systems exhibit multiscale structures, $\ln K$ correlation of such deposits remains poorly understood, limiting the potential application of the theories.

For multiscale deposits, hierarchical analysis have been conducted within a flexible sedimentary framework (Ritzi and Allen-King 1986). Based on indicator transforms, a general formulation is developed to decompose a global variogram across different sedimentary hierarchies. While non-Gaussian $\ln K$ histogram with multiple modes is revealed, the shape of the variogram depends on conductivity contrast and cross-transition probabilities of facies units. By analyzing outcrops, Dai et al. (2005) illustrates the non-uniqueness of hierarchical decomposition and the benefit of using "soft" lithological data to complement limited measurements. Though significant insights have been obtained, they are yet to be tested against datasets that exhibit a wide range of heterogeneities. However, the cost involved in completely characterizing natural deposits by detailed measurements is prohibitive. Outcrop studies are limited by the extent of rock exposure, which can introduce biases in estimating the key statistics (facies proportion, average width/length, within-unit univariate statistics).

In this study, a high-resolution hydraulic conductivity map is created by scaling up an experimental stratigraphy (Fig. 1(a)). Compared to many synthetic aquifers, this conductivity map is unique. The heterogeneity pattern corresponds to physical sedimentation that is statistically inhomogeneous. Heterogeneity exists at multiple scales, organized within a hierarchical framework. Earlier studies conducted geostatistical and upscaling analysis on this map to estimate effective flow and transport parameters (Zhang et al. 2005, 2006; Zhang and Gable 2008). The relevant statistics/parameters apply to individual depositional units for which statistical homogeneity is more or less satisfied (i.e., small $\ln K$ variance). This requirement on weak heterogeneity is necessary to apply the classical stochastic results pertaining to stationary medium.

In recent years, however, a variety of new theories have been developed for non-stationary media of high variance with multiscale or hierarchical structures (Rubin 2003). These theories are not restricted to stationary problems, so a potentially wider range of applications is possible. In particular, Dai et al. (2004) predict solute macrodispersion in multiscale media within a hierarchical geostatistical framework.

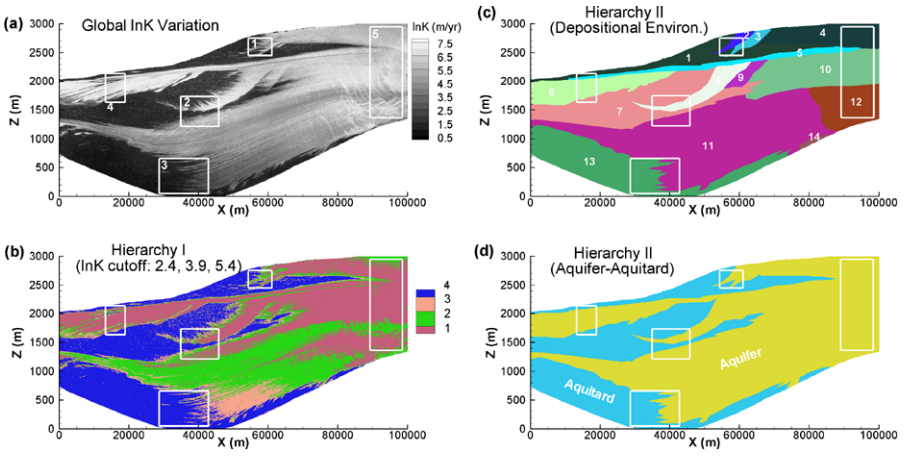

Fig. 1 (**a**) Basin-scale conductivity ($\ln K$) map with sample locations (boxes); (**b**) Indicator value at Hierarchy-I: 1: sand; 2: silty sand; 3: clayey silt; 4: clay; (**c**) Indicator value at Hierarchy-II: 1–14, each represents a facies unit; (**d**) Alternative indicator value at Hierarchy-II: aquifer and aquitard, representing facies assemblage

The relation between macrodispersion and parameters of the component auto- and cross-variograms is explored. Along this inquiry, this study conducts a hierarchical analysis for the experimental stratigraphy, by evaluating select samples from the map, each encompassing multiple depositional environments. Specifically, the traditional (continuous-type) $\ln K$ variogram is decomposed across indicator units defined at two hierarchies (Fig. 1(b), (c), (d)). Unlike our previous studies, consideration of statistical homogeneity is no longer relevant. Any region of the map can be subjected to the analysis.

Since hierarchical division is non-unique, alternative indicator maps are created based on either $\ln K$ cutoffs (Hierarchy-I) or facies types (Hierarchy-II). These schemes of division are similar to those of Dai et al. (2005). To compare results with field observations, both horizontal and vertical variograms are computed. Three questions need to be answered. Can indicator divisions based on conductivity cutoffs reveal the underlying deposition mechanisms? Given exhaustive sampling and alternative hierarchical division, what is controlling the global variogram structure of each sample? How does the different hierarchical division impact the decomposition characteristics? In the following sections, we briefly introduce the experimental stratigraphy and the creation of the indicator maps. We then present the formulations for the hierarchical analysis. Results are presented for 5 select samples. Insights gained are discussed. Finally, results are summarized and future work indicated.

2 Conductivity Map and Hierarchical Division

A high-resolution image is taken of a deposit created in an experimental flume where multiple sedimentary facies formed in response to diverse depositional processes

(Paola 2000). The image is scaled up to sedimentary basin dimensions by assuming appropriate length scales (Δx, Δz) for each pixel or a representative elementary volume (REV). Each REV is assumed homogeneous and isotropic for which a log-linear relation is used to assign a scalar $\ln K$ based on pixel gray scale and representative end-member conductivities. The resulting $\ln K$ map has mean, variance, and frequency distribution comparable to an alluvial fan. It exhibits both global sand/clay transitions and local variations unique to the depositional processes, e.g., long-range stratifications, growth faults, complex spatial trends. More details on the sediment experiment and the assumptions employed to generate the conductivity map can be found in Zhang et al. (2005).

2.1 Hierarchy-I Based on Conductivity Cutoffs

The histogram of the conductivity ($\ln K$) map is multi-modal (Fig. 2). Three conductivity cutoffs can be identified, corresponding to transitions between 4 normal densities fit to the histogram. Four indicator categories are defined and named as: sand ($\ln K > 5.4$), silty sand ($3.9 < \ln K < 5.4$), clayey silt ($2.4 < \ln K < 3.9$), and clay ($\ln K < 2.4$). Due to the log-linear interpolation, these cutoffs are related to the changes in gray scale intensity, thus sand content of the physical stratigraphy. The conductivity ranges of the 4 categories correspond to those of fine to medium sand ("sand"), silt to fine sand ("silty sand"), silt ("clayey silt"), and the more permeable type of clay ("clay") (Freeze and Cherry 1979).

Under this division, an indicator map of the lowest hierarchy (Hierarchy-I) is created (Fig. 1(b)). It reveals global variations between sand-rich fluvial deposit and clay-rich marine deposit while most of the heterogeneities are concentrated in the former. Within the lower fluvial deposit (the corresponding region is unit 11, Fig. 1(c)), complex spatial trends exist, indicating shifts in dominant deposition mode. In partic-

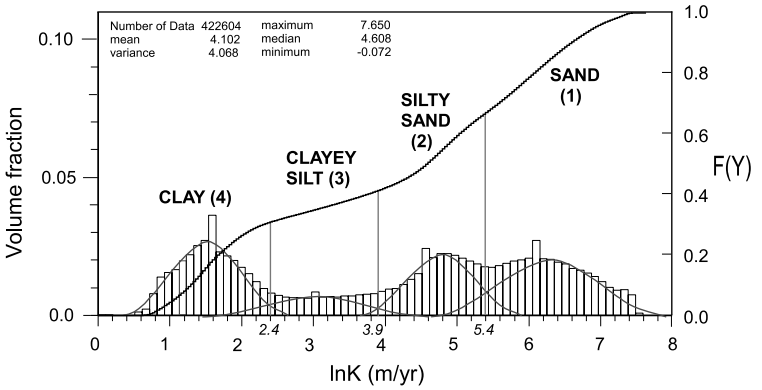

Fig. 2 $\ln K$ histogram and its cumulative distribution function F(Y) for the full map. Univariate statistics are shown near the top. Three $\ln K$ cutoffs are identified, dividing the map into 4 Hierarchy-I categories: sand (I = 1), silty sand (I = 2), clayey silt (I = 3), and clay (I = 4). The corresponding indicator map is shown in Fig. 1(**b**)

ular, in the lower 1/3 of this region, there are lateral changes towards the distal flume from sand (I = 1), to silty sand (I = 2), to clayey silt (I = 3). This strip of deposit formed during tectonic quiescence, streams deposited coarse-grained sediments upstream and carried fine-grained sediments downstream. The indicator map based on ln K cutoffs thus reveals subtle differences in heterogeneity as a result of the changing sediment transport mode.

2.2 Hierarchy-II Based on Facies Types

For the Hierarchy-II division, two alternative definitions are made. Based on depositional environment, various facies can be identified for which the map is divided into 14 units, or Depositional Hierarchy (DH) (Fig. 1(c)). The delineation is based on visual inspection of either the stratigraphic contacts or changes in the dominant heterogeneity style. Units 4, 5, and 10 are designated as fluvial units; units 2, 3, 8, 9 are shoreline; unit 6 is turbidite; units 11, 12 are fluvial/floodplain; and units 1, 7, 13, 14 are deepwater marine deposits. Though units 11 and 12 were both created by fluvial processes, they are separated by a fault. In this case, differences in the subsidence rate along the flume basement (to emulate tectonic subsidence) plays a role.

At the larger facies assemblage scale, an alternative 2-unit division is created (Fig. 1(d)). The aquifer is the sand-rich units of the DH hierarchy combined; the aquitard is the clay-rich units combined. This division is termed as Aquifer–Aquitard Hierarchy (AAH) since it reflects the hydrogeological characteristics of the deposits. The above DH and AAH divisions reflect the zonation approach in creating hydrogeological framework models (Zhang et al. 2006). Similar to Hierarchy-I, all units dividing the space are non-overlapping; unlike Hierarchy-I, Hierarchy-II division is not based on conductivity magnitude. Depending on the underlying processes, each unit may contain high, low, bimodal or multimodal conductivities. The above divisions are non-unique, as alternative or refined divisions are possible. The current choice is made to be consistent with past upscaling work.

2.3 Sample Selections

For the hierarchical analysis, 5 samples are selected based on the following three criteria (Fig. 1). (1) Each samples a different region of the K map, ranging from upstream to downstream. (2) Each samples multiple depositional environments, e.g., fluvial and marine. (3) Observed stratification in each sample ranges from flat to inclined, offering various facies juxtaposition and heterogeneity style. Furthermore, to facilitate interpretation, sample selection aims to incorporate only a modest level of complexity. In general, each sample exhibits a two-level hierarchy, appropriate for the three-level decomposition conducted in this study. For example, sample 4 is observed to contain two dominant hierarchies: between the low-energy deepwater clay and high-energy turbidite, and, within the turbidite, between channel and interbeds. For

Sample ID	N_x	N_z	Continuous Type	Indicator Type		
				Hierarchy I	Hierarchy II	
					Depositional	Aquifer-Aquitard
Sample 1	68	61	Sample Composite Variogram	1,2,3,4	1, 2, 3	Aquit (1); Aquif (2, 3)
Sample 2	108	105			7, 8, 11	Aquit (7); Aquif (8, 11)
Sample 3	142	124			11, 13	Aquit (13); Aquif (11)
Sample 4	57	101			1, 5, 6, 7	Aquit (1, 7); Aquif (5, 6)
Sample 5	93	315			4, 5, 10, 12	Aquif (4, 5, 10, 12)
			Figure 1a	*Figure 1b*	*Figure 1c*	*Figure 1d*

Fig. 3 Sample sizes (N_x, N_z) and indicator values of the associated hierarchies. For the Aquifer–Aquitard Hierarchy, inclusive facies units are shown in parenthesis

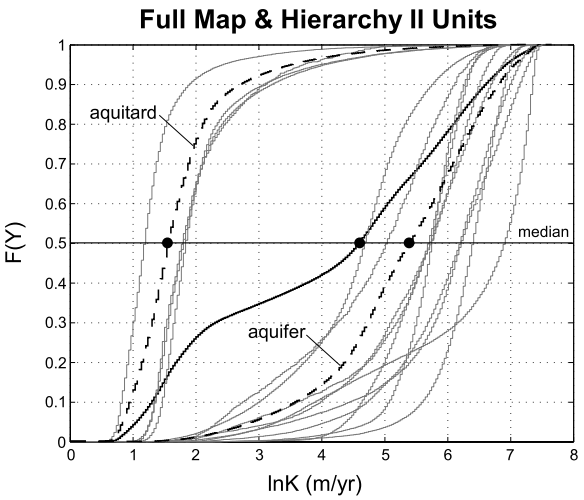

Fig. 4 Cumulative ln K distribution of the full map (*black*) and the Hierarchy-II constituent units (*gray*: DH; *black dashed*: AAH). Median ln K (*solid circles*) are shown for the full basin and the aquifer and aquitard

all samples, the number of data points used, relevant divisions and indicator values are given in Fig. 3.

3 Hierarchical Univariate Analysis

Cumulative ln K distribution (cdf) is computed for the full map as well as for each of the Hierarchy-II constituent units (Fig. 4). The cdf reveals a global bimodal distribution of clay-rich and sand-rich deposits. Similar observations are made when analyzing natural aquifers at facies assemblage scale (Ritzi et al. 2000). The DH units cluster around the respective aquifer or aquitard, corresponding to finer division at the facies scale. However, the cutoff-based Hierarchy-I division exhibits multimodal distribution (Fig. 2). Clearly, the characteristics of the histogram modes depends on the choice of the hierarchical division.

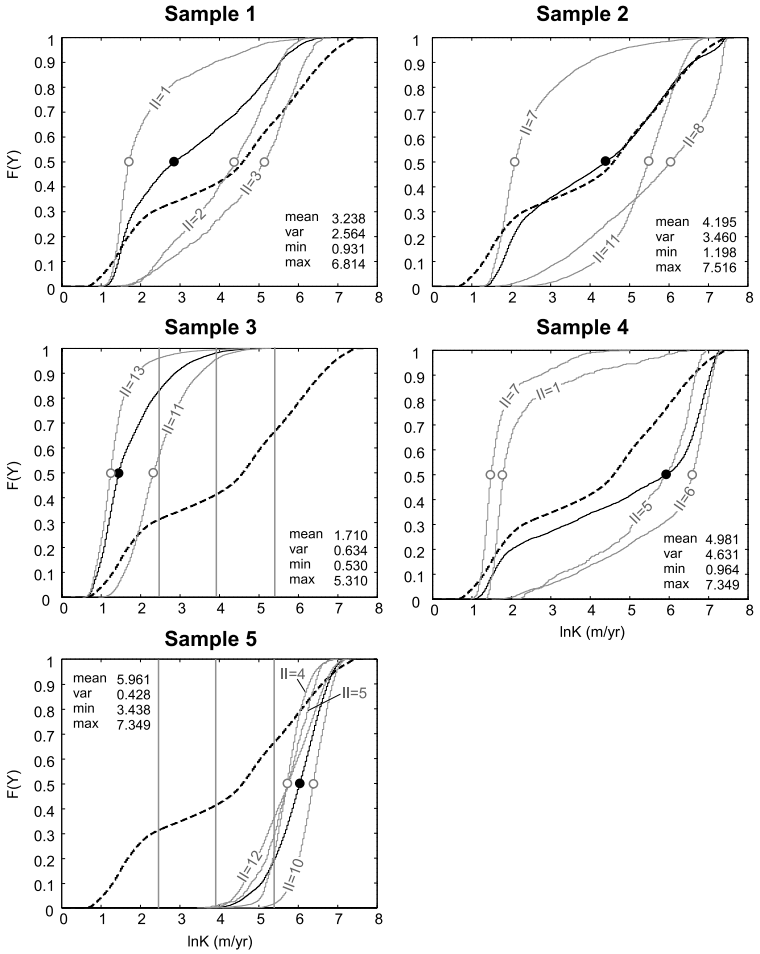

Fig. 5 Cumulative distribution of each sample (*black*) and its constituent DH units (*gray*). The distribution of the full map is shown (*dashed line*). The median ln K is also shown (*solid circle*: full sample; *empty circle*: DH unit) along with select sample statistics. In samples 3 and 5, ln K cutoffs for Hierarchy-I division are indicated as *vertical lines*

The cdf is also computed for each sample and its constituent Hierarchy-II units (DH division) (Fig. 5). For samples that contain both fluvial and marine deposits (e.g., 1, 2, 3, 4), distinct modes exist in medians, separating the cdf of a DH unit from that of the full sample. For samples that contain only fluvial deposits (i.e., 5), the differences among the cdfs are smaller, reflecting similar underlying processes. Similar modes also exist for the aquifer–aquitard division (not shown). Moreover, when compared to the cdf of the full map, samples 1, 2, 4 have similar range and distributional characteristics, but not samples 3 and 5. This has implications for the following hierarchical variogram analysis.

4 Hierarchical Variogram Analysis

4.1 Mathematical Formulations

For each sample, both horizontal and vertical experimental variograms are computed to evaluate the spatial structure of $\ln K$. Each directional variogram is calculated with the classical estimator

$$\gamma_Y(h) = \frac{1}{2N(h)} \sum_{k=1}^{N(h)} \big[Y(x_k) - Y(x_k + h)\big]^2, \tag{1}$$

where $Y = \ln K$; h is the lag separation in a given direction; $N(h)$ is the number of data pairs separated by h; x_k is the coordinate position (for vertical variogram, $x_k = z_k$). (1) calculates a sample composite variogram irrespective of the hierarchical division.

A three-level decomposition is conducted in this study based on two hierarchical divisions: cutoff-based categories (Hierarchy-I); facies- or facies-assemblage-based units (Hierarchy-II). A hierarchical indicator variable is defined as

$$I_{or}(x) = \begin{cases} 1, & \text{if } x \text{ occurs in Hierarchy-I category } r \text{ \& Hierarchy-II unit } o; \\ 0, & \text{otherwise,} \end{cases} \tag{2}$$

where x is the position along the 1D axis; r is the index of categories in Hierarchy-I; o is the index of units in Hierarchy-II. The marginal probability of $I_{or}(x)$ is

$$p_{or} = E\big[I_{or}(x)\big] = \Pr\big[I_{or}(x) = 1\big], \tag{3}$$

where p_{or} represents volume fraction of region or. Thus, $\sum_o \sum_r p_{or} = 1$. Using this indicator variable in a variogram analysis (tail: $I_{or}(x)$; head: $I_{ji}(x + h)$), a transition probability $t_{or,ji}(h)$ is defined (Dai et al. 2004)

$$t_{or,ji}(h) = \Pr\big[I_{or}(x) = 1 \;\&\; I_{ji}(x + h) = 1\big] \big/ \Pr\big[I_{or}(x) = 1\big], \tag{4}$$

where o, j represent Hierarchy-II unit type(s) where tail and head of a data pair fall, respectively; r, i represent Hierarchy-I category type(s) where tail and head fall, respectively. For the divisions adopted in this study, $o, j = 1, \ldots, 14$ (DH), or $o, j = 1, 2$ (AAH); $r, i = 1, \ldots, 4$. Equation (1) can then be expressed as a sum of component variograms, proportions, and transition probabilities (Dai et al. 2005)

$$\begin{aligned} \gamma_Y(h) = & \sum_o \sum_r \gamma_{or,or}(h)\, p_{or}(h)\, t_{or,or}(h) \\ & + \sum_o \sum_r \sum_{i \neq r} \gamma_{or,oi}(h)\, p_{or}(h)\, t_{or,oi}(h) \\ & + \sum_o \sum_{j \neq o} \sum_r \gamma_{or,jr}(h)\, p_{or}(h)\, t_{or,jr}(h) \\ & + \sum_o \sum_{j \neq o} \sum_r \sum_{i \neq r} \gamma_{or,ji}(h)\, p_{or}(h)\, t_{or,ji}(h), \end{aligned} \tag{5}$$

where $\gamma_{or,ji}(h)$ is the sample component variogram for transition between unit types or and ji; $p_{or}(h)$ is the proportion of unit type or for a given h; $t_{or,ji}(h)$ is the sample transition probability from unit types or to ji. The above relation is an exact decomposition of (1) (Ritzi et al. 2004).

To improve interpretability and to reduce the number of statistics that can be presented, each summation in (5) is rewritten using a proportion term which weights a respective component variogram

$$\begin{aligned}\gamma_Y(h) &= \gamma_{\alpha\alpha}(h)P_{\alpha\alpha}(h) + \gamma_{\alpha x}(h)P_{\alpha x}(h) + \gamma_{x\alpha}(h)P_{x\alpha}(h) + \gamma_{xx}(h)P_{xx}(h) \\ &= \gamma^w_{\alpha\alpha}(h) + \gamma^w_{\alpha x}(h) + \gamma^w_{x\alpha}(h) + \gamma^w_{xx}(h), \end{aligned} \tag{6}$$

where $\gamma_{\alpha\alpha}$, $\gamma_{\alpha x}$, $\gamma_{x\alpha}$, γ_{xx} are the same component variograms of (5). A new set of subindexes is used to represent the type of summation which satisfies a specific transition rule: $\gamma_{\alpha\alpha}$ ($\alpha\alpha$ term) includes all autotransition pairs with head and tail falling in the same Hierarchy-I and -II unit; $\gamma_{\alpha x}$ (αx term) includes cross-transition pairs with head and tail in the same Hierarchy-II unit, but different Hierarchy-I units; $\gamma_{x\alpha}$ ($x\alpha$ term) includes pairs with head and tail in different Hierarchy-II units, but the same Hierarchy-I unit (in this study, each Hierarchy-I unit is characterized with a normal density, head and tail falling in the same unit has the same expected value, $\gamma_{x\alpha}$ is thus considered an autotransition term). γ_{xx} (xx term) includes cross-transition pairs with head and tail in different units at both hierarchies. By definition, $P(h) = \sum\sum\sum\sum p_{or}(h)t_{or,ji}(h)$ (Dai et al. 2005). At a given lag, $P_{\alpha\alpha}$, $P_{\alpha x}$, $P_{x\alpha}$, P_{xx} represent proportions of data pairs that satisfy the specific transition rules among all pairs. Thus, $\sum P = 1$ for all lags.

Since hierarchical decomposition is linear, it suggests that the composite variogram shape is controlled by the shapes of the component variograms and their respective proportions. For ease of visualization, the composite variogram is plotted along with the weighted component variograms: $\gamma^w_{\alpha\alpha}$, $\gamma^w_{\alpha x}$, $\gamma^w_{x\alpha}$, γ^w_{xx}, each corresponding to a summation term in (5) or each is a fraction of the total variogram. To evaluate the above exact relations, only horizontal and vertical variograms are computed, eliminating the need for search envelopes. Since the sample data is of regular spacing, the variogram lag is defined as an integer multiple of a unit lag: Δx (horizontal), Δz (vertical). The maximum lag spacing is one half of the sample horizontal or vertical dimension. For each lag, there are thousands to tens of thousands of data pairs, therefore no confidence interval is calculated for the variograms.

4.2 Composite Variogram

The composite variogram is computed for all samples (Figs. 7–11). Due to exhaustive sampling, most variograms are smooth-varying. Compared to variograms computed from field data, irregular local fluctuations do not occur, suggesting that variogram structures are due to deposit variability rather than variogram uncertainty. The composite variograms exhibit exponential, "hole effect", periodic, or nested structures. For a two-level hierarchy, Ritzi et al. (2004) relate the global variogram to the statistics of the units. It is found that exponential-like variograms result from unit types with contrasting K and large length variance. For the Hierarchy-I categories in this

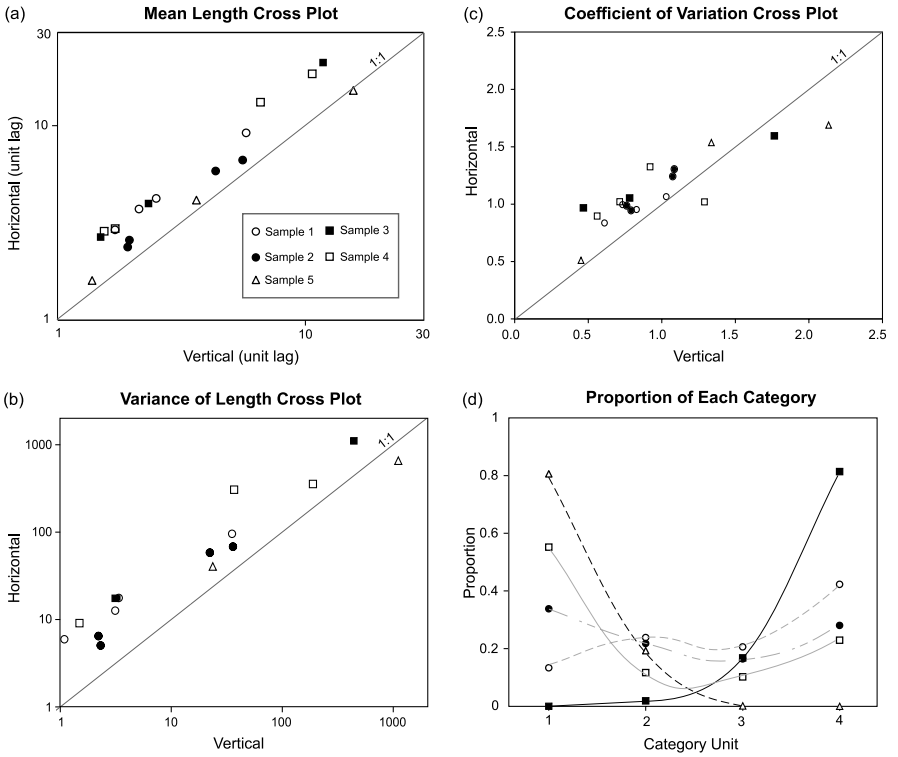

Fig. 6 Statistics of length of each Hierarchy-I category unit, computed for all samples along the horizontal and vertical directions: mean (**a**); variance (**b**); coefficient of variation (**c**). For each category, proportion is also calculated (**d**)

study (different mean K), similar statistics can be computed for each sample (Fig. 6). For most samples, the horizontal mean and variance of the unit length are greater than those of the vertical direction. Compared to the vertical variograms, the horizontal variograms are more exponential-like. Qualitatively, this is consistent with Ritzi et al. (2004). Moreover, the coefficient of variation of the unit length ranges from 0.5 to 2.5 for all samples, indicating a large variability (Fig. 6(c)). The proportion of each category also varies considerably among samples (Fig. 6(d)). Thus, sample selection has captured a wide range of variations in both facies length and proportion.

4.3 Hierarchical Decomposition

Based on the DH Hierarchy, the composite variogram and its component variograms are plotted for all samples (Figs. 7, 8, 9, 10, 11, and 12). The respective proportions are also shown, along with the sum of the appropriate cross terms ($\gamma^w_{\alpha x} + \gamma^w_{xx}$; $P_{\alpha x} + P_{xx}$). Comparing samples, common characteristics are observed along with important exceptions. For all samples, the shape of the composite variogram is determined by the shape of the sum of the cross variograms: $\gamma^w_{\alpha x} + \gamma^w_{xx}$ (or the $\alpha x + xx$ term), consistent with that observed from analyzing an outcrop (Dai et al. 2005). For

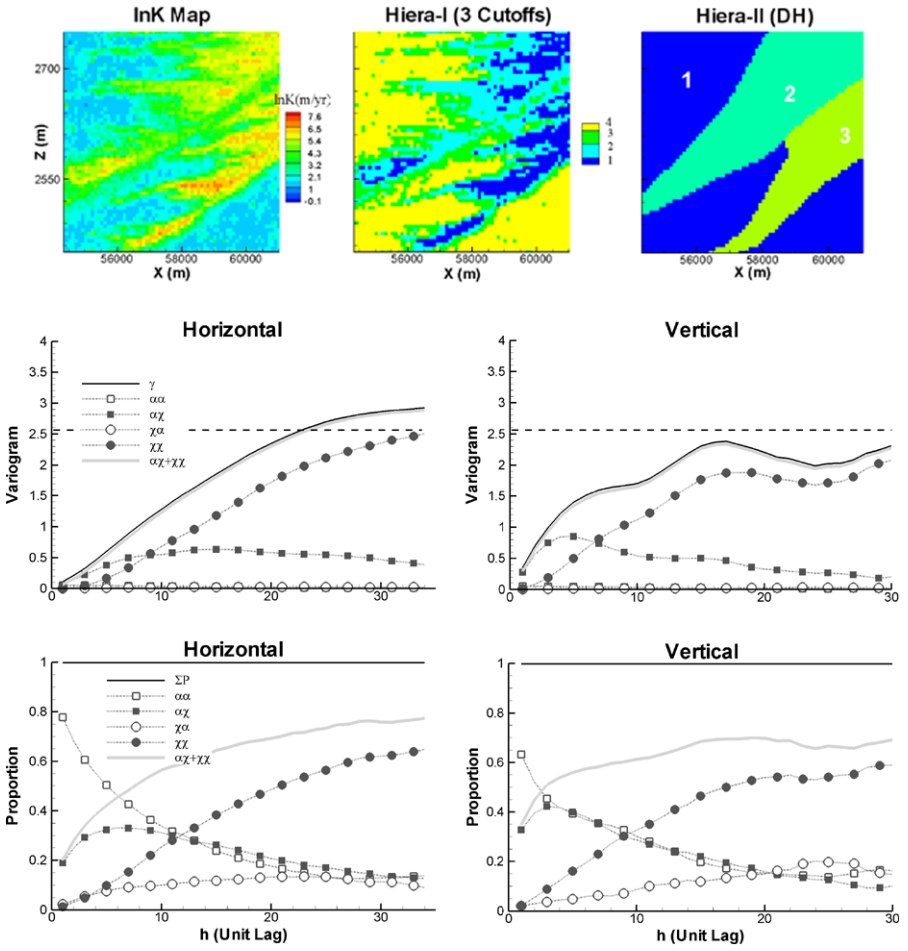

Fig. 7 Hierarchical variograms and respective proportions for sample 1 (DH division): composite variogram: γ; weighted component variograms: $\alpha\alpha$ ($\gamma^w_{\alpha\alpha}$), αx ($\gamma^w_{\alpha x}$), $x\alpha$ ($\gamma^w_{x\alpha}$), xx (γ^w_{xx}); and proportions: $\alpha\alpha$ ($P_{\alpha\alpha}$), αx ($P_{\alpha x}$), $x\alpha$ ($P_{x\alpha}$), xx (P_{xx}). For clarity, only every two point is plotted with symbols while the cross transition terms are those of the filled symbols. The *dashed line* in the variograms is the sample variance. Also shown is the sum of cross terms: $\alpha x + xx$ ($\gamma^w_{\alpha x} + \gamma^w_{xx}$), and the respective proportion ($P_{\alpha x} + P_{xx}$)

samples 1, 2, 4, along both directions, the $\alpha x + xx$ term is nearly identical to the composite variogram. The corresponding proportion ($P_{\alpha x} + P_{xx}$) is large, assigning significant weights to the unweighted component variograms (not shown). Though the proportions of the auto terms ($P_{\alpha\alpha}$, $P_{x\alpha}$) are non-negligible, the magnitudes of the $\alpha\alpha$ and $x\alpha$ component variograms are negligible, indicating that the unweighted variograms are approaching zero. For these samples, the Hierarchy-I categories divide the deposits into units of sufficient internal statistical homogeneity. The within-unit variability is minimal at all scales resulting in negligible auto terms compared to the cross terms.

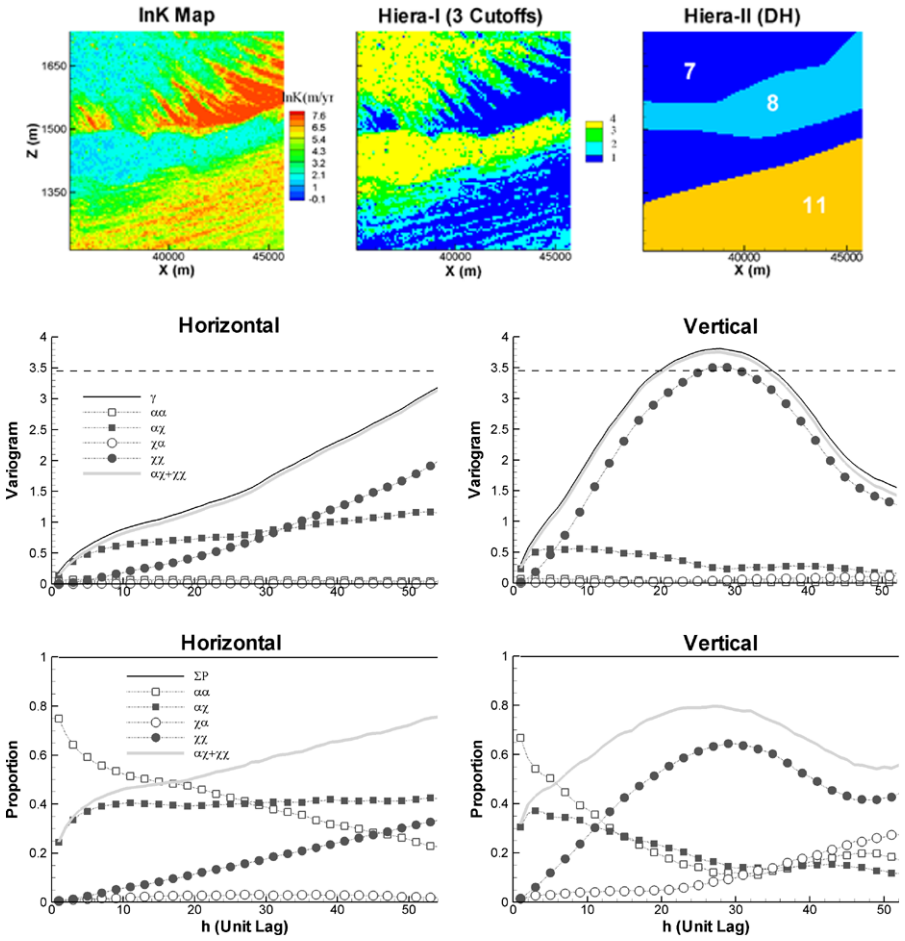

Fig. 8 Hierarchical variograms and proportions for sample 2 (DH division)

However, for samples 3 and 5, in both directions, the sum of the cross variograms is appreciably smaller than the composite variogram. For all samples, $\ln K$ cutoffs are selected from the histogram of the full map. Such a choice minimizes the auto-variograms of samples 1, 2, 4 because their cdfs do not deviate significantly from the global cdf (Fig. 5). The cdfs of samples 3 and 5 deviate from the global cdf. Under the current division, both samples are actually divided into 2 categories. This division is apparently insufficient to minimize the auto terms. For these samples, a more detailed division at the Hierarchy-I level should reduce the auto-variograms. Additional analysis is conducted using 3 cutoffs selected from each sample histogram: 25th, 50th, and 75th percentiles. The recomputed component variograms and their proportions have been significantly adjusted. Only those of sample 5 are shown (Fig. 12), to be compared to Fig. 11. For both samples and both directions, $\gamma^w_{\alpha\alpha}$ and $\gamma^w_{x\alpha}$ have diminished to near zero and the proportion of the cross terms has increased considerably. As a result, the composite variogram is again closely matched by the sum of the

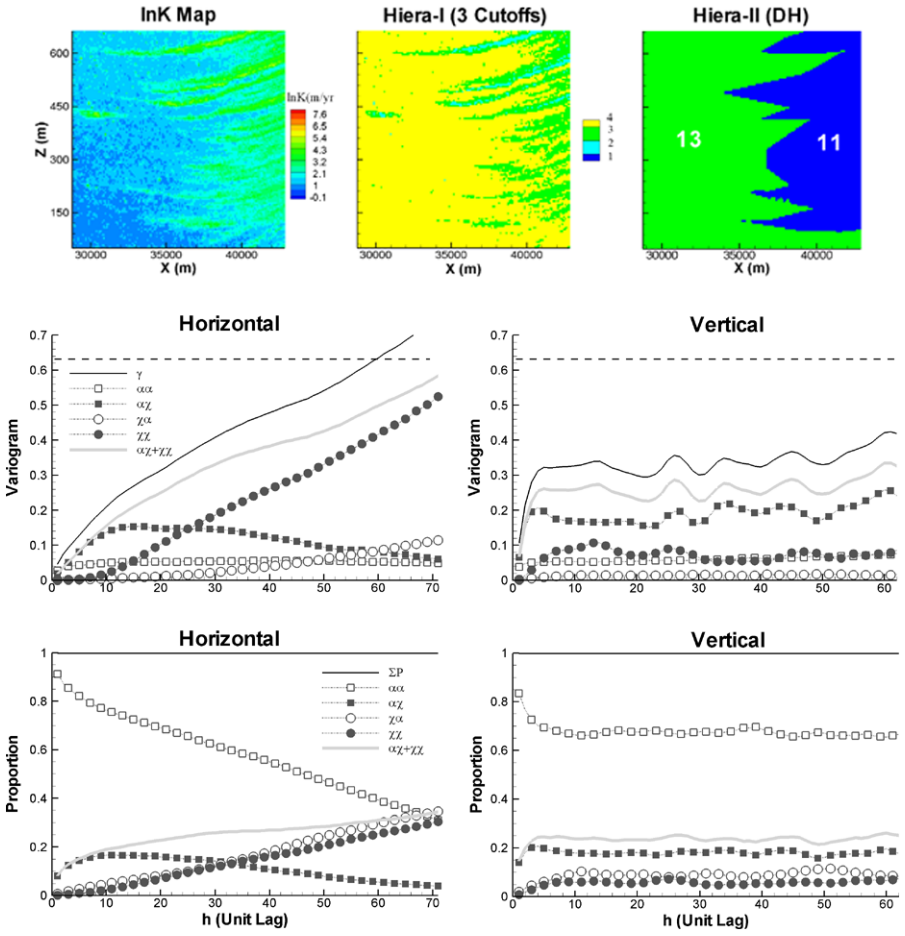

Fig. 9 Hierarchical variograms and proportions for sample 3 (DH division)

cross-transition component variograms, similar to that observed for samples 1, 2, 4. For the given hierarchy, decomposition characteristics are sensitive to the division based on conductivity cutoffs. To minimize the auto terms, 3 cutoffs based on sample statistics appear adequate.

In terms of the $x\alpha$ variogram, it is negligible for all except the horizontal variogram of sample 3 (Fig. 9) and vertical variogram of sample 5 (Fig. 11). For both samples, it is significant due to the coarsely defined facies contact at the Hierarchy-II level. A more detailed mapping that honors the Hierarchy-I divisions should reduce the magnitude of the $x\alpha$ variogram. Moreover, for most samples, the shape of the composite variogram is dominated by the shape of the xx variogram. The horizontal γ_{xx}^{w} of samples 4, 5 is insignificant due to the corresponding low proportion. Few pairs satisfy the xx transition. For the other samples, partial sampling across Hierarchy-II units can provide insights on the *shape* of the global correlation structure. To capture

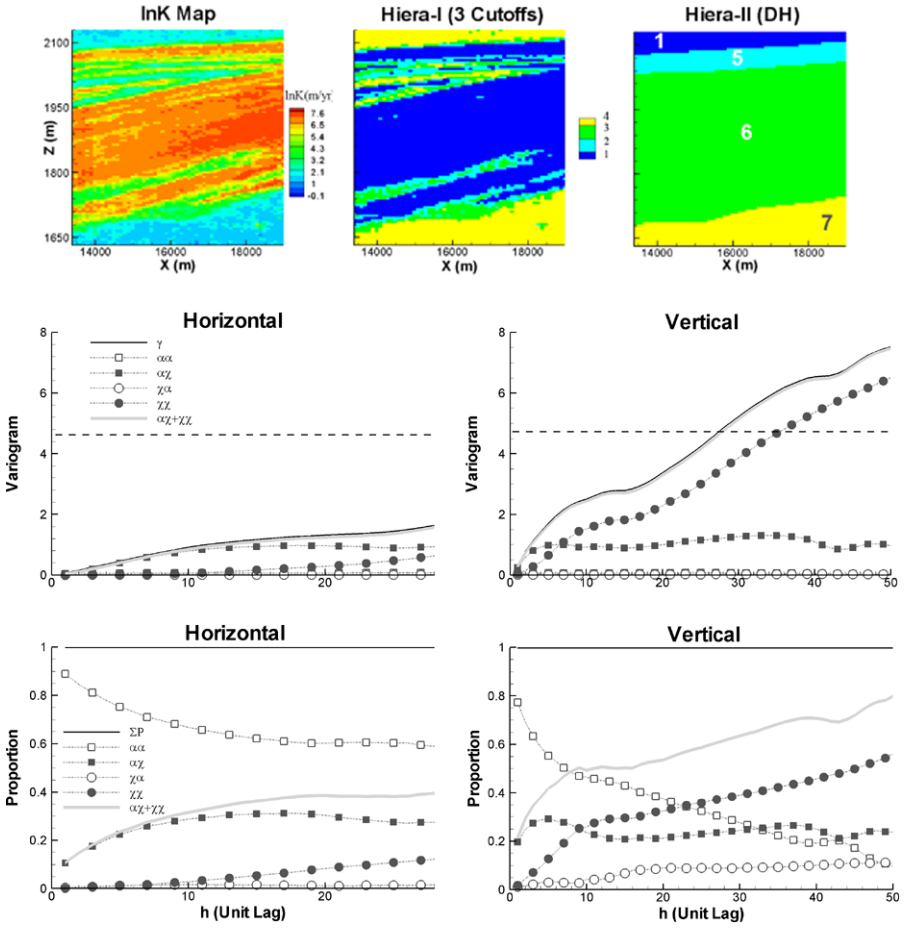

Fig. 10 Hierarchical variograms and proportions for sample 4 (DH division)

the composite sill (as discussed above), both xx and αx variograms are needed; the later requires sampling within each facies unit.

Finally, under the alternative AAH division at Hierarchy-II and the same Hierarchy-I division (all samples using the global cutoffs defined in Fig. 2), the above analysis for each sample is repeated. Compared to DH division, little change occurred in the decomposition characteristics of each sample, along both directions (Fig. 13). This suggests that for the given conductivity map, the AAH (facies assemblage scale) is sufficient to define a Hierarchy-II division. Furthermore, a facies-based sub-division is not necessary. An exception, however, is the vertical variogram of sample 5. In this case, γ_{xx}^{w} is eliminated since only one Hierarchy-II unit (aquifer) is defined. No pairs can be found satisfying the xx transition. The old xx pairs (of the DH division) are added to the αx term, so the relationship between the composite variogram sill and the sum of the cross-transition component variograms remains the same.

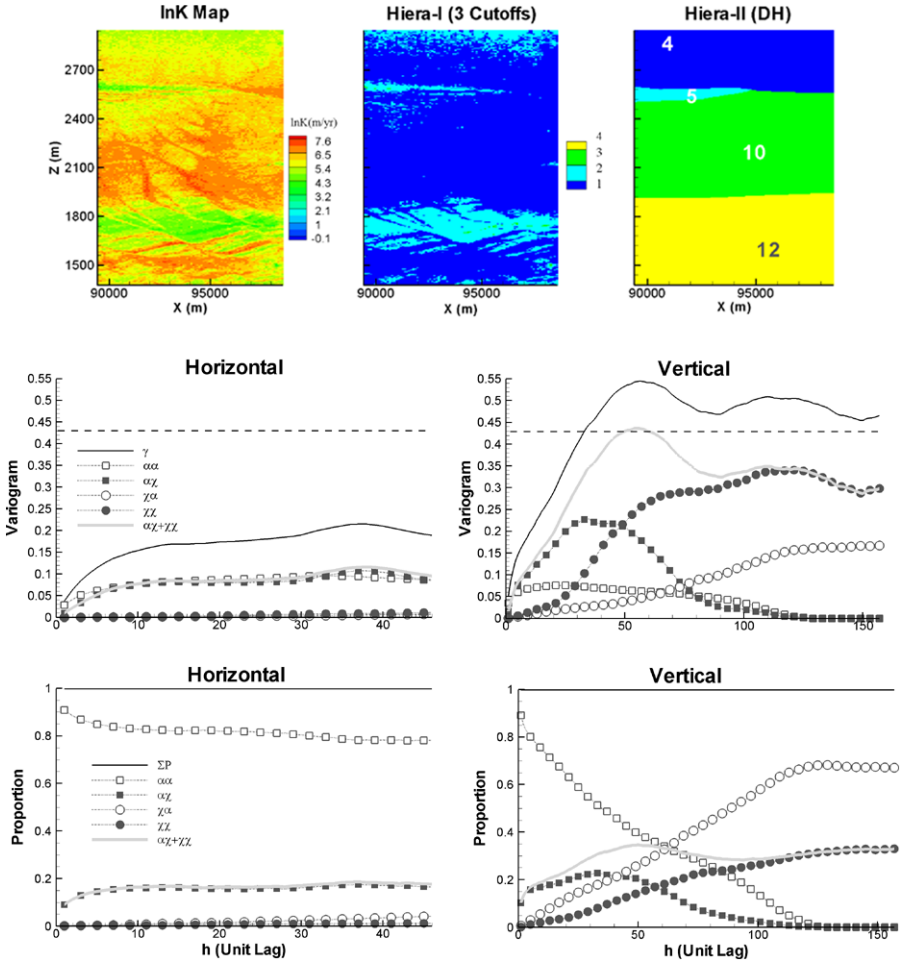

Fig. 11 Hierarchical variograms and proportions for sample 5 (DH division)

5 Summary and Conclusions

Based on an experimental stratigraphy, this study conducts a hierarchical geostatistical analysis on selected samples, each incorporating multiple depositional environments. Three indicator-based hierarchical divisions are defined: 4 categories based on conductivity cutoffs (Hierarchy-I), 14 unit types based on facies types (Hierarchy-II DH), and 2 unit types based on facies assemblage types (Hierarchy-II AAH). Along both horizontal and vertical directions, sample composite variogram and its auto- and cross-transition component variograms are calculated. The decomposition characteristics are then evaluated against the underlying heterogeneity and specific division rule.

Given the diverse heterogeneity and the facies relation evaluated, results suggest that (1) $\ln K$ cutoffs (i.e., sand contents) can be used to distinguish shifts in domi-

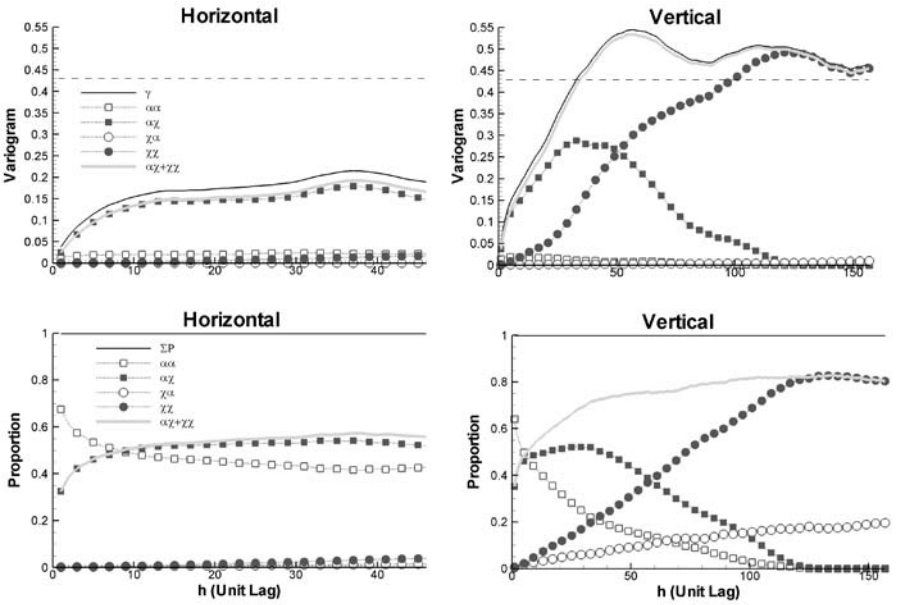

Fig. 12 Hierarchical variograms and proportions for sample 5 (DH division), based on new ln K cutoffs: 25th, 50th, and 75th percentiles of the sample histogram

nant deposition mode; (2) Sample univariate modes depend on the choice of hierarchical division; (3) Sample composite variograms exhibit smooth-varying structures that are consistent with the prediction for a two-level hierarchy (Ritzi et al. 2004). Exponential-like variograms are observed in samples with a large variance in mean facies length. (4) The decomposition characteristics are sensitive to the division based on conductivity cutoffs (Hierarchy-I categories with different mean K), but are not sensitive to the division based on depositional environment (Hierarchy-II facies and facies assemblage types). 3 ln K cutoffs, appropriately defined, appear to reduce the importance of the auto terms to zero, resulting in a composite variogram dominated by the cross-transition component variograms. (5) At the Hierarchy-II level, the AAH division gives similar decomposition characteristics as the DH division. In light of the fact that decomposition is sensitive to the conductivity-based cutoffs, the mean conductivities of these units defined at both scales are not significantly different. For this conductivity map, parsimony in hierarchical division is achieved at the facies assemblage scale.

By eliminating local parameter uncertainties, the experimental stratigraphy can provide a deterministic framework to develop a sampling strategy in multiscale media (or obtain univariate and bivariate statistics for the facies units based on limited sampling). This is important for effective parameter estimation using classical theories (Zhang et al. 2006; Zhang and Gable 2008). The samples and the hierarchical statistics analyzed in this study can provide parameters to test alternative, non-stationary theories. The ultimate goal is to understand how flow and transport should be modeled in geologically realistic, multiscale deposits. Thus, the merits and limitations of

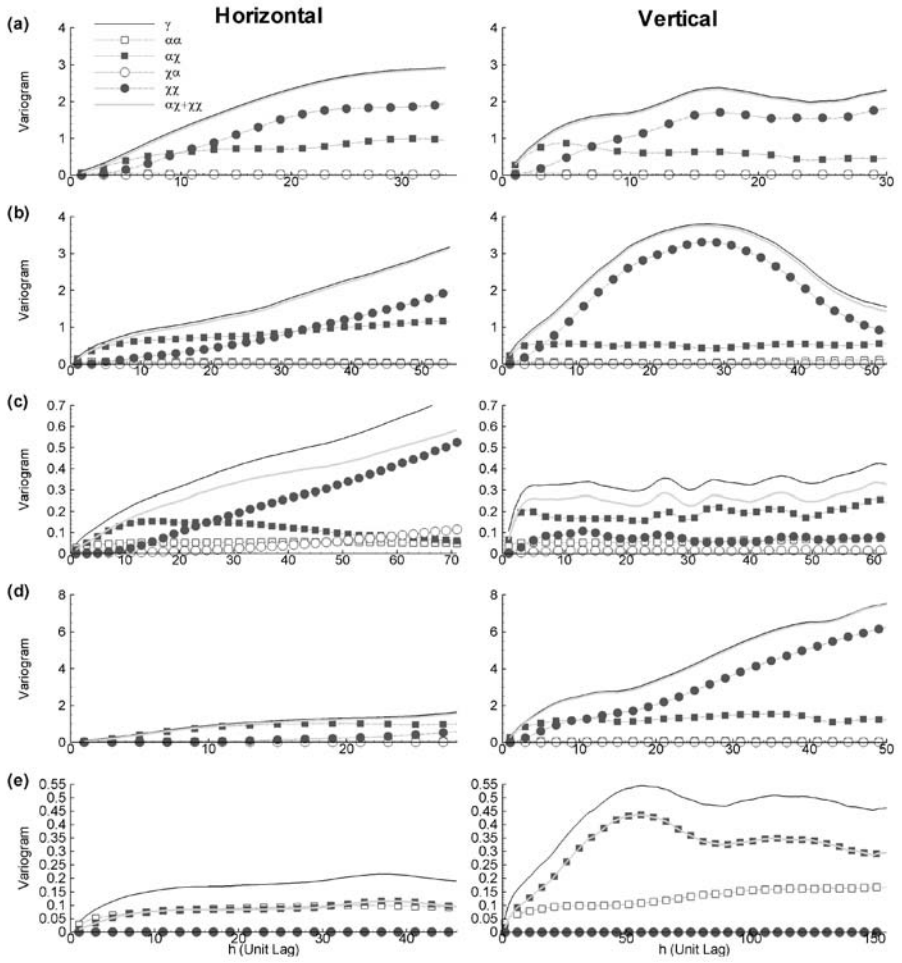

Fig. 13 Hierarchical variograms for samples 1–5 (**a**)–(**e**), respectively, based on the AAH division

the classical (stationary) approaches will be compared in future to alternative non-stationary methods. In the experimental flume, deposits possessing finer scale sedimentary structures have also been created. Future work will consider the geostatistics of these deposits which can be compared to field characterizations of natural alluvium (which the experiment attempts to emulate). Such efforts will reveal the fundamental links between hierarchical geostatistics, upscaling characteristics, and multiscale sedimentary heterogeneity in three dimensions.

Finally, it is important to note that variogram-based geostatistics has its limitations. In the reservoir simulation community, higher order statistical approaches (multiple point statistics (MPS)) have been developed to represent curvilinear geobodies that honor the observed correlations among multiple points in space (Strebelle 2002; Ortiz and Deutsch 2004). Combined with the reservoir modeling workflow, geologically realistic simulation models are developed using MPS to populate the

petrophysical properties in important flow units (Milliken et al. 2007). Real subsurface data is rarely detailed enough to allow MPS to make the necessary inferences. Instead, training images are used to depict geological heterogeneities that are expected for a particular depositional setting. A 3D experimental stratigraphy has indeed been built which can provide a training image from which multidimensional statistical correlations can be extracted for MPS simulations. This will be pursued in the future.

Acknowledgements The work is supported by the Turner Postdoc Fellowship of the Department of Geological Sciences, University of Michigan. The author acknowledges the helpful communications with Dr. Robert Ritzi. The comments of two anonymous reviewers have helped to improve the contents of this work.

References

Dai Z, Ritzi RW, Huang C, Rubin YN, Dominic DF (2004) Transport in heterogeneous sediments with multimodal conductivity and hierarchical organization across scales. J Hydrol 294:68–86

Dai Z, Ritzi RW, Dominic DF (2005) Improving permeability semivariograms with transition probability models of hierarchical sedimentary architecture derived from outcrop analog studies. Water Resourc Res 41:W07032. doi:10.1029/2004WR003515

Freeze AR, Cherry JA (1979) Groundwater, 1 edn. Prentice Hall, New York

Milliken W, Levy M, Strebelle S, Zhang Y (2007) The effect of geologic parameters and uncertainties on subsurface flow: deepwater depositional systems. SPE, 109950

Ortiz JM, Deutsch CV (2004) Indicator simulation accounting for multiple-point statistics. Math Geol 36(5):545–565

Paola C (2000) Quantitative models of sedimentary basin filling. Sedimentology 47:121–178

Ritzi RW et al (2000) Comparing statistical models of physical heterogeneity in buried-valley aquifers. Water Resourc Res 36(11):3179–3192

Ritzi RW, Dai Z, Dominic DF, Rubin Y (2004) Spatial correlation of permeability in cross-stratified sediment with hierarchical architecture. Water Resourc Res 40:W03513. doi:10.1029/2003WR002420

Ritzi Jr RW, Allen-King RM (2007) Why did Sudicky (1986) find an exponential-like spatial correlation structure for hydraulic conductivity at the Borden research site. Water Resourc Res 43:W01406. doi:10.1029/2006WR004935

Rubin Y (2003) Applied stochastic hydrogeology. Oxford University Press, London

Strebelle S (2002) Conditional simulation of complex geological structures using multiple-point statistics. Math Geol 34(1):1–21

Zhang Y, Gable CW (2008) Two-scale modeling of solute transport in an experimental stratigraphy. J Hydrol 348(3–4):395–411

Zhang Y, Person MA, Paola C, Gable CW, Wen X-H, Davis JM (2005) Geostatistical analysis of an experimental stratigraphy. Water Resourc Res 41:W11416. doi:10.1029/2004WR003756

Zhang Y, Gable CW, Person M (2006) Equivalent hydraulic conductivity of an experimental stratigraphy: implications for basin-scale flow simulations. Water Resourc Res 42:W05404. doi:10.1029/2005WR004720